ORIGINAL CONTRIBUTION

Analysis of the flow behavior of electrorheological fluids containing polypyrrole nanoparticles or polypyrrole/silica nanocomposite particles

Youngwook P. Seo[1] · Sangsok Han[1] · Jihun Kim[1] · Hyoung Jin Choi[2] · Yongsok Seo[1]

Abstract

A four-parameter model (Seo-Seo model) was used to analyze the flow behavior of some electrorheological (ER) fluids containing polypyrrole (PPy) nanoparticles, nanocomposite particles of conductive polypyrrole confined in mesoporous silica (MCM-41), and core-shell-structured SiO_2/polypyrrole nanoparticles. The static yield stress predictions by the model were compared with the experimental data and dynamic yield stress obtained from the Bingham model and/or Cho-Choi-Jhon (CCJ) model. The static yield stress values were larger than the dynamic yield stress values. It was also found that the static yield stress of the polypyrrole suspension had a quadratic dependence on the electric field strength as predicted by the electric polarization model whereas those of the nanocomposite suspensions showed 1.5 power-law dependency. A master curve describing the yield stress data dependence on the electric field strength was obtained using a single-parameter scaling function to interpret the underlying mechanism of ER activity. A simple method for evaluating the activity mechanism criterion has been proposed and applied to the ER response of those three kinds of suspension. The results show that the critical electric field strength should be checked before the conduction mechanism is asserted, even if the yield stress plot shows 1.5 power-law dependence on the electric field strength.

Keywords Static yield stress of ER fluid · Seo-Seo model · ER activity mechanism · Critical electric field strength

Introduction

Electrorheological (ER) fluids typically consist of polarizable particles in an electrically insulating fluid (Seo and Seo 2012; Seo et al. 2012; Dong et al. 2019). When an electric field induces attractive interactions between the polarizable particles, these particles form a solid-like network of fibril shapes within a few milliseconds oriented along the direction of the electric field. Reverse transition occurs as soon as the electric field is switched off. In ER fluids, shear deformation leads to yield stress mainly because of two interactions: electrostatic interactions between the suspended ER particles and hydrodynamic interactions. At low shear rates ($\dot{\gamma}$), the electrostatic interactions between the suspended ER particles induced by the external electric field dominate the hydrodynamic interactions and thus lead to the formation of aggregated fibril structures (mesostructures). These fibril structures hinder the flow of the suspension, leading to yield stress before the flow starts. At high shear rates, however, the hydrodynamic interaction dominates. The fibril structures of ER fluids completely collapse, resulting in liquid-like behavior, in which the yield stress (τ_y) follows a power-law dependency on the electric field strength (E) such as $\tau_y \propto E^{1.5 \sim 2}$ (Seo and Seo 2012; Seo et al. 2011; Kim et al. 2016). These features lead to remarkable changes in the rheological properties of the fluid which shows wide potential applications such as dampers, brakes, shock observers, drug delivery, and robotics (Zhang et al. 2009; Yamaguchi et al. 2010).

Youngwook P. Seo and Sangsok Han contributed equally to this work.

✉ Hyoung Jin Choi
hjchoi@inha.ac.kr

✉ Yongsok Seo
ysseo@snu.ac.kr

1 Department of Materials Science and Engineering, College of Engineering, RIAM, Seoul National University, Seoul 08826, South Korea

2 Department of Polymer Science and Engineering, Inha University, Incheon 22212, South Korea

Although many ER devices have been successfully manufactured, more effective ER fluids with higher yield stress and reduced power consumption operating at a low electric field are demanded for their further applications and commercialization. Considerable efforts have been made in recent years to improve the performance of the ER fluid, for example, by coating the suspended particles with electrically active polymers or by preparing composite particles (Armes 1996). Polypyrrole (PPy) is one of the most promising semi-conducting materials because it exhibits excellent physical properties such as high electrical conductivity, polarizability, and stability. Therefore, PPy and its composite materials are frequently used in the preparation of efficient ER materials (Cheng et al. (2006a, b); Kim and Kim 2007; Sedlačík et al. 2012; Fang et al. 2013). Some years ago, Cheng et al. (2006a) reported an anhydrous ER fluid prepared by dispersing nano-composite particles of conducting PPy and mesoporous silica (MCM-41) in the silicone oil. The PPy was synthesized in an aqueous solution of $FeCl_3 \cdot H_2O$ after the pyrrole monomer was introduced into the mesoporous silica (MCM-41) channels prior to the polymerization; thus, it was confined in the silica (MCM-41) channel. Choi et al. analyzed the ER properties of mesoporous PPy/MCM-41 suspensions later (Cho et al. 2004; Liu and Choi 2009). Recently, Kim et al. 2016 also investigated the ER properties of a core-shell-structured SiO_2/PPy nanoparticle suspension of which structure is opposite to Cheng et al.'s nanoparticles. Silica nanoparticles were modified by 3-(trimethoxysilyl)propyl methacrylate and a conducting PPy shell was then synthesized on the modified silica surface via oxidative polymerization with $FeCl_3$ as the oxidant. To be used as an ER material, the SiO_2/PPy particles were controlled by a dedoping process where 1 M NaOH was added to the particle suspension until the pH value reached 10 (Kim et al. (2016)). In both studies, the yield stress was dependent on the electric field, following the 1.5 power-law behavior. Thus, the ER activity mechanism was asserted to follow the conduction model as suggested by Davis and Gender (Davis and Ginder 1995). On the other hand, Goodwin et al. synthesized the PPy particles of 260 nm in diameter for the preparation of electrorheological (ER) fluids in dodecane (Goodwin et al. 1997). The particles were stabilized by a graft copolymer with poly(12-hydroxystearic acid) as the stabilizing moieties. An AC electric field at 50 Hz was applied to the fluids using field strengths up to 1 kV mm^{-1} and the viscometric behavior was examined. The PPy suspensions exhibited Bingham behavior and the fluid behavior could be calculated from the interparticle polarization forces. The dependence of the Bingham yield stress on the electric field strength is E^2. Slightly higher values of the power-law index at lower volume fractions were possibly due to greater uncertainty in the fit of the shear stress-shear rate curves (Goodwin et al. 1997). At low volume fractions and low field strengths, the stress decreased slightly (~ 5%) at the lowest shear rates,
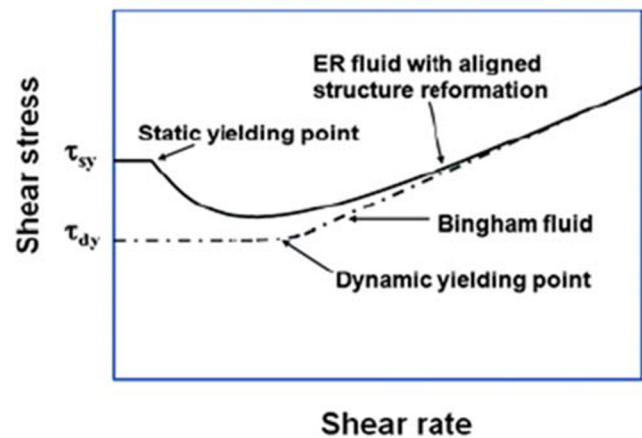
Fig. 1 Schematic figure of the flow curve (broken line) for the Bingham fluid and (solid line) ER fluid. τ_{sy} is the static yield stress while τ_{dy} is the dynamic yield stress (Seo and Seo 2012)

which led to increased uncertainty in the fit. The weaker the ER effect, the more doubtful the existence of static yield stress. On the other hand, it was shown that the change in viscosity with shear rate scales with the Mason number, Mn, which expresses the ratio between polarization forces and shear forces (Parathasarathy and Klingenberg 1996). The pure PPy particle suspension shows different ER activity mechanism following the polarization model than that of two nano-composite particle suspensions which were supposed to follow the conduction model.

In this study, we reanalyzed the experimental data of those three reports by using the Seo-Seo model (Seo and Seo 2012) to evaluate the static yield stresses (τ_{sy}) instead of the dynamic yield stresses (τ_{dy}) and to clarify the flow behavior of these ER fluids as well as the mechanism of the ER reaction. The static yield stresses were compared with the experimental data and the dynamic yield stresses (τ_{dy}) obtained with the Bingham and/or CCJ models (Cheng et al. 2006a, b; Liu and Choi 2009; Kim et al. 2016). The underlying ER mechanism was reconsidered by examining the nonlinear dependence of the static yield stress on the electric field strength (Davis and Ginder 1995; Wu and Conrad 1996).

Rheological models for the yield stress

As already mentioned, there are two yield stresses in ER fluids: the static yield stress (τ_{sy}) and the dynamic yield stress (τ_{dy}) (Fig. 1) (Seo and Seo 2012; Méheust et al. 2011). The dynamic yield stress (τ_{dy}) is obtained by extrapolating the shear stress curve versus the shear rate to the zero shear rate (Seo et al. 2018; Choi et al. 2014). The Bingham model is the simplest model to fit the yield flow behavior; the relationship between the shear stress (τ) and the shear rate ($\dot{\gamma}$) is as follows

$$\tau = \tau_{dy}(E) + \eta_{pl}\dot{\gamma}, \quad \tau \geq \tau_0(E) \tag{1}$$

$$\dot{\gamma} = 0, \quad \tau < \tau_0(E) \tag{2}$$

where $\tau_{dy}(E)$ is the dynamic yield stress when the electric field strength is E, and η_{pl} is E-dependent plastic viscosity, which approaches the suspension viscosity at a sufficiently high shear rate (Seo et al. 2018). Since the Bingham model does not adequately account for the structural change in the ER fluid during flow, Choi et al. proposed an empirical alternative model (Cho-Choi-Jhon (CCJ) model), which is a variation of the Bingham model that takes into account such structural changes (Cho et al. 2004),

$$\tau = \frac{\tau_{dy}}{\left(1 + \left(t_1 \dot{\gamma}\right)^{\alpha}\right)} + \eta_{\infty}\left(1 + \frac{1}{\left(t_2 \dot{\gamma}\right)^{\beta}}\right)\dot{\gamma} \tag{3}$$

where t_1 and t_2 are time constants, $\dot{\gamma}$ is the shear rate, τ_{dy} is the dynamic yield stress, and η_{∞} is the viscosity at high shear rates.

The yield stress of the ER fluid is the minimum stress that causes a shear flow in the undisturbed fluid state at rest (Parmar et al. 2008) The fibril-shaped structures are destroyed and the ER fluid flows when the shear stress exceeds the electric field forces that hold the fibril aggregates together. The shear stress of the flow decreases with the shear rate, but the broken structures tend to regroup to regain the aligned mesostructures because of the electrical dipoles between the particles. However, the shear stress of the fluid decreases after such reformation because the reformed structures are not as complete as those that were originally formed before the start of the shear flow process (Seo and Seo 2012; Seo et al. 2014)). The dynamic yield stress values obtained with the Bingham model are strongly influenced by the shear rate range, but are less affected when they are obtained with the CCJ model (Cho et al. 2005). When the stress value passes through a minimum during the structural change, the dynamic yield stress may or may not reach the minimum stress value depending on the depth of the minimum at which the fibril structure completely disintegrates under the continuous shearing (Seo et al. 2015).

On the other hand, the static yield stress, τ_{sy}, is the yield stress required for a static ER fluid to flow. The Seo-Seo model was used to calculate the static yield stress that met the yield criterion and to model the stress changes associated with the structural realignment (Seo and Seo 2012; McIntyre et al. 2013; Han et al. 2018).

$$\tau = \tau_{sy}\left(1 - \frac{\left(1 - \exp\left(-a\dot{\gamma}\right)\right)}{\left(1 + \left(a\dot{\gamma}\right)^{\alpha}\right)}\right) + \eta\dot{\gamma} \tag{4}$$

where τ_{sy} is the static yield stress, η is the shear viscosity, a is the time constant (i.e., the reciprocal of critical shear rate for the deformation of 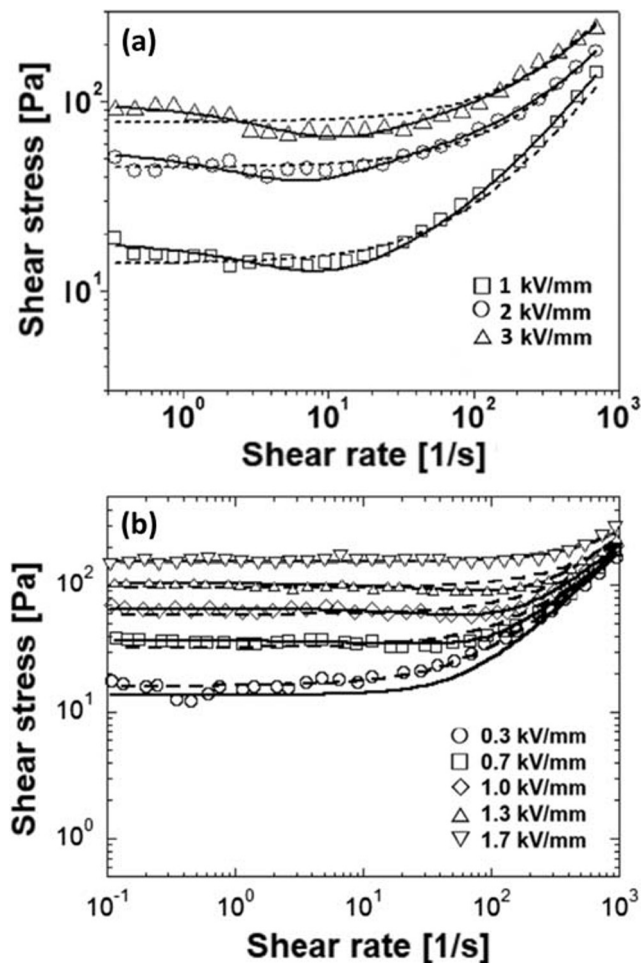the aligned particle structure), and α is the power-law index used to assess the degree of shear thinning (Seo and Seo 2012; Seo et al. 2014). This model has been shown to adequately account for the variation in the stress change with the shear rate described by the Papanastasiou model (Papanastasiou 1987; Seo and Seo 2012; Seo et al. 2012; McIntyre et al. 2013). Another advantage is that other models for predicting the dynamic yield stress can be included in the Seo-Seo model by varying the parameter values, for example, a Newtonian fluid ($\tau_{sy} = 0$), the Bingham fluid ($a = 0$), the De Kee-Turcotte model ($\alpha = 0$, $a \neq 0$), and the Herschel-Bulkley model ($a = 0$, $\eta = m\dot{\gamma}^{n-1}$) (Seo and Seo 2012). The Seo-Seo model is suitable to predict the static yield stress of magnetorheological (MR) fluids as well as that of ER fluids (Seo et al. 2018).

After the yield stresses are obtained for different electric field strengths, the particle aggregation mechanism is related to the yield stress on the electric field strength. The yield stress (τ_y) of an ER fluid is known to exhibit a non-analytic power-law dependence on the electric field strength (E_0), $\tau_y \propto E_0^m$ (Davis 1992; Parmar et al. 2008; McIntyre et al. 2013). The τ_y dependence can be divided into two regions by the critical electric field strength, E_c: $\tau_y \propto E_0^2$ for $E_0 < E_c$ because of the particle polarization and $\tau_y \propto E_0^{3/2}$ for $E_0 > E_c$ due to the electrical breakdown of ER fluids under high electric field strength (Davis 1992; Davis and Ginder 1995; Wu and Conrad 1996; Choi et al. 2001). The critical electric field strength, E_c, depends on several factors such as the particle conductivity, the conduction mismatch between the particle and the medium liquid, and the particle volume fraction (Choi et al. 2001; Wu and Conrad 1996). Since a number of factors affect the value of E_c, the decision of E_c should be done before deciding the mechanism. Here, we propose a simple method to decide the E_c based on the two different fitting methods of the experimental data. Seo proposed a simple nonlinear equation that can fit the yield stress master curve after scaling of the electric field strengths,

$$\tau_{sy}(E_0) = \alpha' E_0^{3/2}\left(1 - exp\left(-m'\sqrt{E_0}\right)\right) \tag{5}$$

where m' is a fitting parameter. This equation yields two limiting behaviors of the yield stress at low and high electric field strengths, i.e., at low electric field strengths, $\tau_{sy} \propto E_0^2$ for $E_0 << E_c$ and $\tau_{sy} \propto E_0^{1.5}$ for $E_0 >> E_c$ (Seo 2011). Though it is an empirical equation, we have demonstrated that it fits the ER fluids yield stress behavior quite well (Seo et al. 2012, 2018). Normalizing with E_c and using $\tau_{sy,\,0} = \alpha' E_c^{3/2}$ give the following universal fitting equation,

$$\hat{\tau} = \hat{E}^{3/2}\left(1 - \exp\left(-m\sqrt{\hat{E}}\right)\right) \tag{6}$$

where $\widehat{\tau} = \tau/m_1 E_c^{m_2}$ and $\widehat{E} = E/E_c$. Both the upper and lower power-law fits should meet at $\widehat{E} = 1$ and $\widehat{\tau} = 1$. The non-dimensional equation Eq. (6) should satisfy this condition, too. Then, E_c value can be approximately determined from Eqs. (6) and (8),

$$\alpha' E_c^{3/2}\left(1 - exp\left(-m'\sqrt{E_c}\right)\right) = m_1 E_c^{m_2} \tag{9}$$

Modeling results and discussion

The experimental data for the PPy/ mesoporous MCM-41 particle suspensions of Cheng et al. (Cheng et al. 2006a, b; Liu and Choi 2009) were reanalyzed first by using the Bingham model, Eq. (1), and the Seo-Seo model, Eq. (4). The shear stress curves are replotted as a function of the shear rate in Fig. 2a. At a high shear rate ($\dot{\gamma}$), the predictions of the Bingham model are in good agreement with the experimental stress values. However, at lower shear rates, there are significant differences from the actual stress values. The flow curves display the ER fluid dynamics of the rupture and reformation of the aligned structures: the flow curve exhibits a significant stress decrease with recovery due to structural changes (Seo and Seo 2012). This demonstrates that the Bingham model is difficult to explain the ER suspension's deformation, breakup, and realignment of fibril networks at low shear rate. On the other hand, hydrodynamic forces tend to destroy the ER structures and promote flow at high shear rates (Seo et al. 2018; Parmar et al. 2008). As the shear rate increases, the effects of the hydrodynamic forces are expected to dominate the effects of the electrostatic forces (Kim et al. 2016; Seo et al. 2015). The ER fluid is then completely broken down with no chainlike structure, and it behaves as a shear thinning fluid

Fig. 2 a Flow curves of shear stress vs. shear rate for PPy /MCM-41-based ER fluids at 1 kV/mm (square), 2 kV/mm (circle), 3 kV/mm (triangle) for Seo-Seo model (solid line) and for Bingham model (3-point dot line). Data from Cheng et al. (2006a). b Flow curves of shear stress vs. shear rate for core-shell-structured SiO$_2$/PPy nanoparticle–based ER fluid at 0.3 kV/mm (circle), 0.7 kV/mm (square), 1.0 kV/mm (diamond), 1.3 kV/mm (triangle), and 1.7 kV/mm (inverted triangle) for Seo-Seo model (solid line) and Bingham model (3-point dot line). Data from Kim et al. (2016))

where $\widehat{\tau} = \tau_y/\alpha' E_c^{3/2}$, $\widehat{E} = E/E_c$, and $m = m'\sqrt{E_c}$. After normalizing the data to produce a single curve, this simple equation was used to fit the static yield stress behavior of the three ER fluids (Figs. 3 and 4b). Excellent agreement was achieved with a single parameter, m, without requiring any arbitrary division in the range of the electric field strength (Seo et al. 2012, 2014). Since the yield stress data can be fit by the power-law model, the half region data (above or below the E_c) can be fit using a single power-law function,

$$\tau_{sy}(E_0) = m_1 E_0^{m_2} \tag{7}$$

Then, after normalization this equation is converted as

$$\widehat{\tau} = \widehat{E}^{m_2} \tag{8}$$

Table 1 The optimal parameters obtained from the flow curves of PPy /MCM-41 (10 wt%) based ER fluid

Model	Parameter	Electric field strength (kV/mm)		
		1	2	3
Seo-Seo	τ_{sy} (Pa)	18.08	57.5	97.42
	η_∞(Pa.s)	0.18	0.20	0.23
	a	0.21	0.18	0.17
	α	0.32	0.40	0.46
Bingham	τ_0 (Pa)	14.0	45.0	78.0
	η_0 (Pa.s)	0.18	0.20	0.26
CCJ[a]	τ_{dy} (Pa)	17.0	48.0	75.0
Experiment[b]	τ_{sy}(Pa)	19.1	50.6	90.0

[a] Cited from Table 1 in Liu and Choi (Liu and Choi 2009)

[b] Cheng et al.'s data (Cheng et al. 2006a)

Table 2 The optimal parameters obtained from the flow curves of core/shell structured SiO$_2$/PPy nanoparticle-based ER fluid

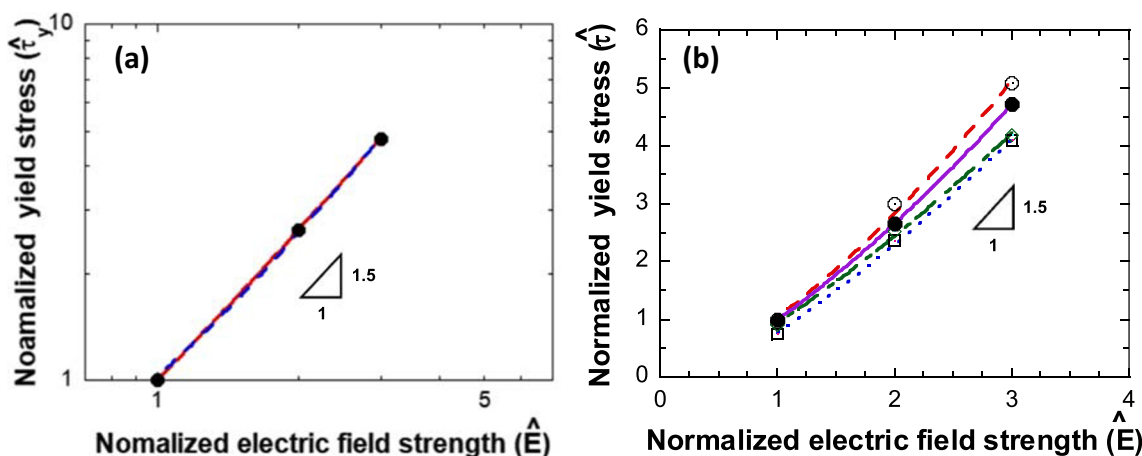| Model	Electric field strength (kV/mm)				
	0.3	0.7	1.0	1.3	1.7
Bingham (τ_{dy})[a] (Pa)	17.6	36.4	64.2	101.0	151.0
CCJ (τ_{dy})[a] (Pa)	18.6	40.4	72.2	111.0	151.0
Seo-Seo (τ_{sy}) (Pa)	13.7	36.6	65.7	102.8	154.8

[a] Cited from Table 1 in Kim et al. (2016)

(Parmar et al. 2008). The results of the Seo-Seo model for PPy/MCM-41-based ER fluids show a good agreement with the experimental shear stress over the entire shear rate range (Fig. 2a).

The dynamic yield stresses are strongly affected by the shear rate range used in the extrapolation and should thus be evaluated as the minimum of the shear stress if the stress value passes through a minimum during the structural change. However, this extrapolation at the minimum of the shear stress means that the breakup and realignment of the fibril network in the low and moderate shear rate region are not adequately considered (Fig. 1). For this reason, the dynamic yield stress, τ_{dy}, is not equivalent to the yield stress of an ER fluid. If the minimum-around region in the stress curve is flat, as in the case of the magnetorheological fluid, the dynamic yield stress value can be close to the static yield stress values (Seo et al. 2018; Choi et al. 2014). On the other hand, the static yield stress for an ER fluid measured under continuous shearing can be significantly different from the dynamic yield stress

because ER fluids are naturally thixotropic due to the destruction of the mesostructure, which resists flow-induced particle rearrangement (Méheust et al. 2011; Seo et al. 2012). The Seo-Seo model takes into account the variation in the shear stress with the shear rate to obtain the static yield stress. The yield stress increases steadily with the electric field strengths (Table 1). In particular, the critical shear rate, which can be expressed as the inverse of the time constant a, $\dot{\gamma}_y^* = 1/a$, is the point where the ER fluids undergo a transition (McIntyre et al. 2013). It increases with the electric field strength which means that the structural change occurs at higher shear rates under the stronger electric field due to the greater cohesion between the particles. The viscosity, η, also increases with the electric field strengths because of the rapid assembly of chains. Table 1 summarizes the values of the dynamic yield stress and the static yield stress. Experimentally, the static yield stress can be measured by using the controlled shear stress (CSS) mode (Han et al. 2018). The static yield stress values predicted by the Seo-Seo model showed excellent agreement with the experimental data (Chuah et al. 2015; Choi et al. 2019).

Likewise, Kim et al.'s report for the flow curves of conductive PPy-coated silica nanoparticles dispersed in silicone oil and their electrorheological (ER) characteristics under electric fields were also analyzed using the Seo-Seo model (Fig. 2b). The core-shell-structured nanoparticles have the opposite structure of the PPy/MCM41 nanocomposite particles, in which PPy is confined in the silica, in the sense that the conducting layer forms the outside. Hence, they show higher yield stress than the PPy/ mesoporous MCM-41 particle suspensions under the same electric field strength because of the

Fig. 3 Normalized static yield stress versus the normalized electric field strength. **a** ER fluid of nanocomposite of PPy confined in mesoporous silica (MCM-41). Straight line is the fit by the power-law model ($\propto E^{1.5}$) and the dotted line is a nonlinear function fit (Eq. (5)). The parameter, m, value was 0.364. **b** ER fluids of core/shell SiO$_2$/PPy nanocomposite particles: static yield stress (white circle) obtained from the Seo-Seo model. Experimental data (black circle), dynamic yield stress from the Bingham model (square), and dynamic yield stress (diamond) obtained from the CCJ model. Lines are the fits using the power-law dependence, Eq. (7). The power-law index is 1.5 for the Seo-Seo model data, 1.42 for the experimental data, 1.32 for the CCJ model data, and 1.31 for the Bingham mode data, respectively. In order to show the power-law dependence and the applicability of Eq. (5), the normalization was done by the lowest value of the electric field strength measured and the stress value there rather than the critical electric field strength
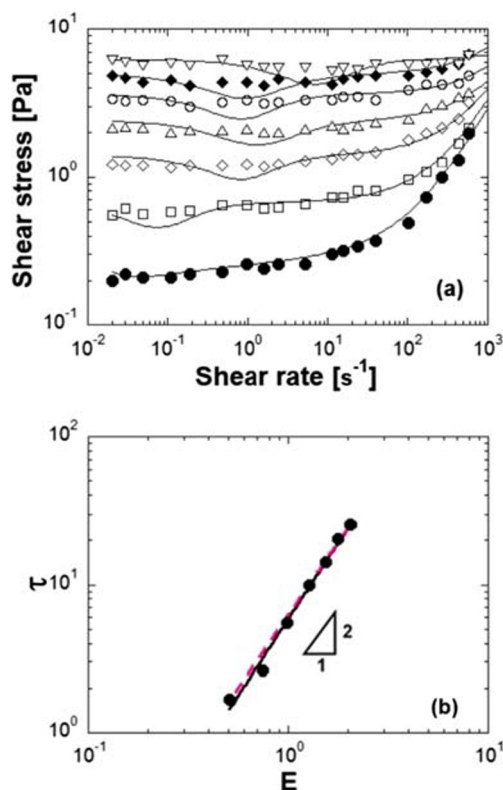
stronger attraction from the higher polarization which is ascribed to the PPy coating (shell) layer (Kim et al. 2016). The Seo-Seo model that takes into account the variation in the shear stress with the shear rate demonstrates again a good agreement with the experimental data. The yield stress also increases steadily with the electric field strengths (Table 2). This suspension exhibits relatively shallow minimum region whereby a close agreement between the dynamic yield stresses from the Bingham model or CCJ model and the static yield stress from the Seo-Seo model is observed (Table 2).

The particle aggregation behavior can be deduced from the dependence of the yield stress on the electric field strength. As previously stated, the τ_y dependence on the electric field strength is divided into two regions by the critical electric field strength, E_c: $\tau_y \propto E_0^2$ for $E_0 < E_c$ because of the particle polarization and $\tau_y \propto E_0^{3/2}$ for $E_0 > E_c$ at high electric field strengths due to the electrical breakdown of ER fluids under high electric field strength (Davis 1992; Davis and Ginder 1995; Wu and Conrad 1996; Choi et al. 2001; Wu and Conrad 1996). However, some uncertainties in the decision of the critical

Fig. 4 a Shear stress as a function of shear rate for PPy. Experimental points are from Goodwin et al. (1997) (200 V/mm (black circle), 300 V/mm (square), 400 V/mm (white diamond), 500 V/mm (triangle), 600 V/mm (white circle), 700 V/mm (black diamond), and 800 V/mm (inverted triangle)) and lines are calculated curves using the Seo-Seo model. **b** Static yield stress of PPy ER fluids versus the electric field strength. Solid line is the fit by the quadratic power-law model ($\propto E^2$), while dotted line is a nonlinear function fit (Eq. (6)). When Eq. (5) was applied, the parameter, m, value was 0.114

electric field strength E_c were not clarified yet (Espin et al. 2006; Parmar et al. 2008; Dong et al. 2019). A plot of the yield stress vs. the electric field strength after normalization is shown in Fig. 3a for the PPy/mesoporous MCM-41 nanocomposite suspensions. The static yield stress values obtained from the Seo-Seo model are close to the experimental data (Table 1).

More importantly, fitting the stress values with the power law is supposed to provide information about the particle aggregation mechanism (Kim et al. 2016; Kim and Kim 2007). The power-law index value, m, of the static yield stress is close to 1.5 according to the Seo-Seo model, which is possibly ascribed to the electrical breakdown of ER fluids if the electric field strength is high (Wu and Conrad 1996; Parmar et al. 2008; Kim and Kim 2007). But its true mechanism might be different from this inference. Obviously, the electric polarization mode, in which the yield stress exhibits a quadratic dependence on the electric field strength, does not appear for the PPy/MCM-41 suspensions due to the poor polarization by the surrounding non-conducting MCM-41 tube (Anderson 1994; Parathasarathy and Klingenberg 1996; Cheng et al. 2006b). The dynamic yield stress results obtained with the Bingham model or CCJ model have even lower power-law index values. Similar yield stress dependency on the electric field strengths for the Kim et al.'s suspension containing core-shell PPy/silica nanocomposite particle is also observed in Fig. 3b. Since this particle's shell is comprised of the PPy, the polarization appears more strongly than the PPy/MCM-41 suspension which can be confirmed in Fig. 3b and Table 2. However, this suspension also shows a similar 1.5 power-law dependency, though dynamic yield stress dependency was lower than that of the static yield stress. Kim et al. presumed the ER activity mechanism to follow the conduction model (Kim et al. 2016), but it can be a hasty conclusion if we take into account of ER behavior of pure PPy particle suspensions.

The ER fluid behavior of pure PPy particle suspensions was reported by Goodwin et al. (Goodwin et al. 1997). Figure 4a shows the flow curves of the PPy ER fluid under various electric field strengths. Although these flow curves do not show the breakage and reforming of the aligned structures evidently due to the low electric field strengths (less than 1 kV/mm), thus, there is only a broad plateau in the shear stress; the static yield stress obtained after fitting the flow curves with the Seo-Seo model increases with the electric field (Fig. 4b). It shows that PPy particle suspension has an apparent quadratic dependence on the electric field strength, which may convincingly demonstrate that the 1.5 power-law dependence of the PPy/MCM-41 ER fluids may not be due to the nonlinear electrical breakdown of the ER fluids under a strong electric field but rather to the weak polarization arising from the confinement of PPy in the mesoporous silica (Goodwin et al. 1997; Choi et al. 2014). Kim et al.'s conclusion on the electrical field strength dependency of the yield stress of core/shell nanoparticle suspension might be

hasty because of uncertainty in other parameters such as the conduction mismatch between the particle and the medium liquid, and the particle volume fraction (Kim et al. 2016). On the other hand, the yield stress values for PPy-coated polyethylene (PE) particle suspension were shown to be proportional to E^2, which is consistent with the expected increase in electrostatic polarization with increasing particle surface conductivity (Anderson 1994; Klingenberg et al. 2007; Davis and Ginder 1995; Kim and Park 2002).

The point here is that assertion of the ER activity mechanism by the yield stress power-law index fit only can mislead the ER activity mechanism unless the basic assumption for the separation of the polarization mechanism range and the conduction mechanism range is ensured (Davis and Ginder 1995; Wu and Conrad 1996; Boissy et al. 1996). In fact, many previous studies did not check the suitability of the ER mechanism (Choi et al. 2014; Dong et al. 2019). By using the proposed method in Eq. (9), the approximate E_c values were obtained as 5.54 kV/ mm for the suspension fluids containing nanocomposite particles of conducting PPy confined in a mesoporous silica (MCM-41), 4.4 kV/mm for the suspension fluids containing core/shell-structured SiO_2/PPy nanoparticles, and 12.29 kV/mm for the PPy nanoparticle suspension fluids. These are much larger than the experimental electric field strengths for all three suspensions. All the electric field strengths are then below the critical electric field strength, E_c, which means the conducting model is not applicable for both nanocomposite particle suspensions. For pure PPy particle suspension fluids, polarization model is applicable and the fitting results correctly correspond to this. Since all ER fluids include many particle simultaneous cohesion, the application of the pairwise particle interaction modeling for the conduction model can be misleading, even if the basic assumption of E_c condition is satisfied (Wu and Conrad 1996). Special attentions should be paid when the yield stress dependence on the electric field strength is smaller than the quadratic dependence though the electric field strength is lower than the E_c; i.e., other factors should be checked before making an assertion on the ER fluid activity mechanism. Goodwin et al. showed that the dependence of the dynamic (Bingham) yield stress on field was E^2 for pure PPy ER fluids at the higher volume fractions. The value of the power index was almost constant ~ 2 (Goodwin et al. 1997).

If the primary forces governing the behavior of ER fluids are electrostatic polarization forces induced by an applied electric field and hydrodynamic forces caused by the particle motion relative to the continuous phase, the non-dimensionalized ER fluid properties should depend only on the ratio of the electrostatic polarization force to the magnitude of the hydrodynamic force (Méheust et al. 2011; Parathasarathy and Klingenberg 1996). The dipole-dipole interactions are proportional to the square of the electric field intensity due to particle polarization, E^2, whereas the shear strength acting on a particle within an ER chain is proportional to the local shear constraint, i.e., the shear
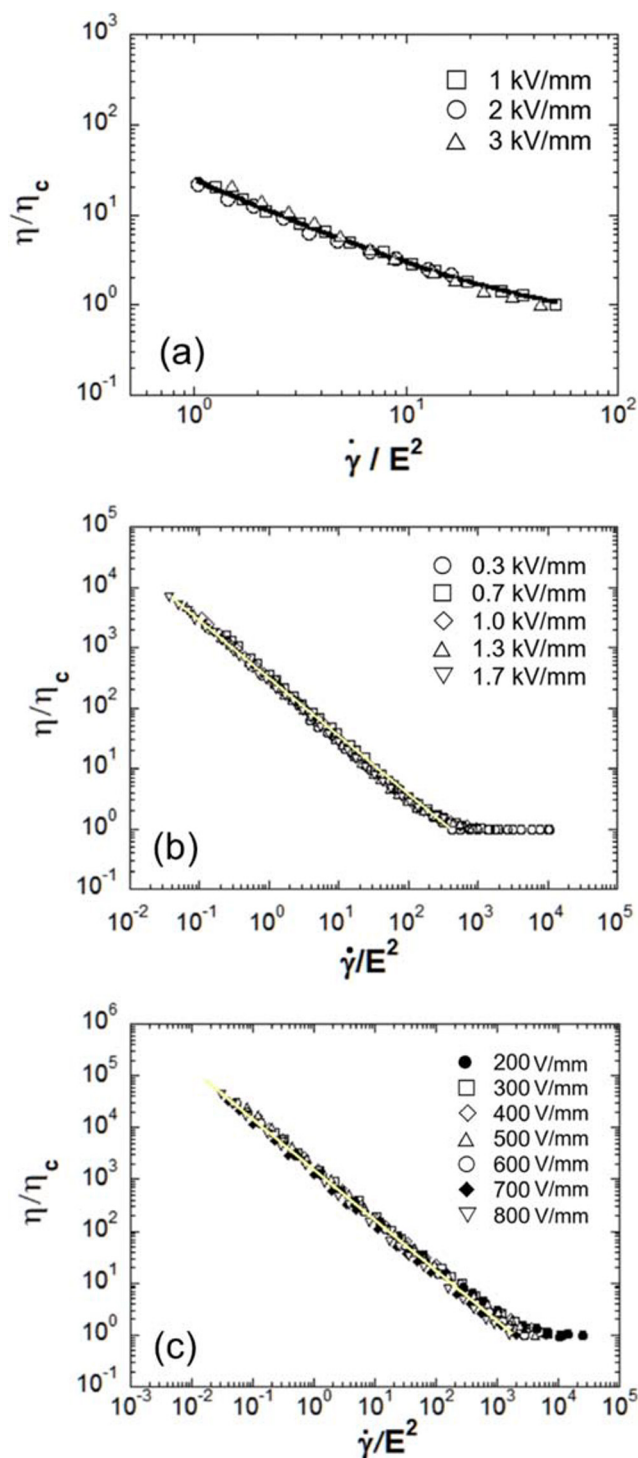
Fig. 5 Normalized viscosity versus the ratio of shear rate $(\dot{\gamma})/E^2$ which is proportional to the modified Mason ratio. All the lines are slope of -1. **a** ER fluids of nanocomposite of PPy confined in mesoporous silica (MCM-41), **b** ER fluids of core/shell SiO_2/PPy nanocomposite particles, and **c** PPy nanoparticle suspension

rate, $\dot{\gamma}$. Hence, the normalized shear that allows for the comparison of the shearing process to the cohesive ER structures present in different runs is $\dot{\gamma}/E^2$, which is proportional to the Mason

number, Mn (Mn $= \mu_0 \gamma / 2\varepsilon_0 \varepsilon_c \beta^2 E^2$, where μ_0 is the medium viscosity, β is the dielectric contrast factor ($= (\varepsilon_p - \varepsilon_c)/(\varepsilon_p + 2\varepsilon_c)$), ε_p is the particle dielectric constant, ε_c is the dielectric constant of the liquid medium phase, and $\varepsilon_0 = 8.854 \times 10^{-14}$ F/cm is the vacuum permittivity) (Parathasarathy and Klingenberg 1996; Méheust et al. 2011). If this reasoning works for the PPy suspensions, then the apparent viscosity η ($= \tau / \gamma$) is proportional to Mn^{-1}, provided the volume fraction of the particle remains constant (Klingenberg et al. 2007). After the non-dimensionalization of the viscosity by dividing it with the viscosity at an electric field strength of zero (η_c) and plotting it as a function of $\dot{\gamma} / E^2$, the dimensionless apparent viscosities should collapse onto a single curve. All three fluid curves show that the log(viscosity) curve vs. log ($\dot{\gamma} / E^2$) has a slope of nearly -1 at small $\dot{\gamma} / E^2$, whereas the curve smoothly approaches unity at large $\dot{\gamma} / E^2$ (Fig. 5). Some scattering of the data is ascribable to the inaccuracy of the measurement due to weak ER effects as well as non-Bingham fluid behavior (Marshall et al. 1989; Klingenberg 2007).

These results validate that the polarization mechanism works for all three particle suspensions at least within the applied electric field strengths. Also, it further elucidates that the low yield stress dependence on the electric field strengths for the nanocomposite particle suspensions is not because of the ER activity mechanism change but rather because of other reasons. Therefore, even if the yield stress plot shows 3/2 power-law dependence on the electric field strengths, we should be certain about the critical electric field strength and the applicability of conduction mechanism for general ER suspensions (Anderson 1994).

its structure was opposite to the PPy/MCM-41 nanocomposite particles and its polarization is much greater.

Although the 1.5 power-law dependence on the electric field strength was observed, this outcome should be distinguished from the prediction of the conduction model, which is considered to be applicable. Unless the condition that the electric field strength is higher than the critical electric field strength (E_c) which is the basic assumption for the conduction model, the 1.5 power-law dependency does not necessarily mean the ER behavior following the conduction model. In the case of the pure PPy nanocomposite particle suspension, the yield stress showed the quadratic dependence on the electric field strength, following the polarization model. We proposed a simple method to calculate the E_c that is a touchstone of differentiating the ER activity mechanisms. The nonlinear one-parameter equation proposed by Seo can be used to fit the universal plot of the static yield stress and to obtain E_c. This means if the electric field strength is lower than E_c, the polarization mechanism works for all three particle suspensions at least within the applied electric field strength range. Flow curve analysis using the Seo-Seo model in combination with dimensional analysis demonstrates to yield proper qualitative and quantitative predictions of ER fluid behaviors with relatively few experimental measurements and to elicit their working mechanism.

Conclusions

In this paper, the flow behavior of electrorheological fluids containing PPy nanoparticles, PPy/silica nanocomposite particles (PPy confined in a mesoporous silica), and core-shell silica-PPy nanocomposite particles was reanalyzed using the Seo-Seo model. The Seo-Seo model convincingly predicted the static yield stress data over the tested range of the electrical field strength. It describes the deformation (breakup and reformation) of aligned structures at low shear rates and the yield flow behavior at high shear rates. The static yield stress of the PPy/MCM-41 nanocomposite ER fluid was found to exhibit a 1.5 power-law dependence on the electrical field strength possibly due to the weak polarization of the nanocomposite particles that arises from the confinement of PPy in the non-conducting mesoporous silica (MCM-41). The suspension of core-shell (silica-PPy) nanoparticle also showed a similar 1.5 power-law dependence on the electrical field strength, though

References

Anderson RA (1994) Electrostatic forces in an ideal spherical-particle electrorheological fluid. Langmuir 10:2917–2928

Armes SP (1996) Conducting polymer colloids. Current Opin Colloid Interf Sci 1:214–220

Boissy C, Atten P, Foulc JN (1996) On the role of conductivities and frequency in the electrorheological effect. J Intel Mater Syst Struct 7:599–603

Cheng Q, Pavlinek V, Lengalova A, Li C, He Y, Saha P (2006a) Conducting polypyrrole confined in ordered mesoporous silica SBA-15 channels: preparation and its electrorheology. Micropor Mesopo Mater 93:263–269

Cheng Q, He Y, Pavlinek V, Lengalova A, Li C, Saha P (2006b) Preparation and electrorheology of new mesoporous polypyrrole/MCM-41 suspensions. J Mater Sci 41:5047–5049

Cho MS, Choi HJ, Ahn WS (2004) Enhanced electrorheology of conducting polyaniline confined in MCM-41 channels. Langmuir 20:202–207

Cho MS, Choi HJ, Jhon MS (2005) Shear stress analysis of a semiconducting polymer based electrorheological fluid system. Polymer 46:11484–11488

Choi HJ, Cho MS, Kim JW, Kim CA, Jhon MS (2001) A yield stress scaling function for electrorheological fluids. Appl Phys Lett 78: 3806–3808

Choi HJ, Zhang WL, Kim S, Seo Y (2014) Core-shell structured electro- and magneto-responsive materials, fabrication and characteristics. Materials 7:7460–7471

Choi J, Han S, Kim H, Sohn E, Choi HJ, Seo Y (2019) Suspensions of hollow polydivinylbenzene nanoparticles decorated with Fe3O4 nanoparticles as magnetorheological fluids for microfluidics applications. ACS Appl Nano Mater 2:6939–6947

Chuah WH, Zhang WL, Choi HJ, Seo Y (2015) Magnetorheology of core-shell structured carbonyl iron / polystyrene foam nanoparticles suspension with enhanced stability. Macromolecules 48:7311–7319

Davis LC (1992) Polarization forces and conductivity effects in electrorheological fluids. J Appl Phys 72:1334–1340

Davis LC, Ginder JM (1995) In: Havelka KO, Filisko FE (eds) Electrostatic forces in electrorheological fluids progress in electrorheology. Plenum, New York, pp 107–114

Dong YZ, Seo Y, Choi HJ (2019) Recent development of electro-response smart electrorheological fluids. Soft Matter 15:3473–3486

Espin MJ, Delgado AV, Plocharski JZ (2006) Effect of additives and measurement procedure on the electrorheology of hematite/ silicone oil suspensions. Rheol Acta 45:865–876

Fang FF, Liu YD, Choi HJ (2013) Electrorheological and magnetorheological response of polypyrrole/magnetite nanocomposite particles. Colloid Polym Sci 291:1781–1786

Goodwin JW, Markham GM, Vincent B (1997) Studies on model electrorheological fluids. J Phys Chem B 101:1961–1967

Han S, Chi J, Seo YP, Park IJ, Choi HJ, Seo Y (2018) High-performance magnetorheological suspensions of pickering- emulsion-polymerized polystyrene/Fe3O4 particles with enhanced stability. Langmuir 34:2807–2814

Kim DH, Kim YD (2007) Electrorheological properties of polypyrrole and its composite ER fluids. J Ind Eng Chem 13:879–894

Kim YD, Park DH (2002) The electrorheological responses of suspensions of polypyrrole-coated polyethylene particles. Colloid Polym Sci 280:828–834

Kim MW, Moon IJ, Choi HJ, Seo Y (2016) Facile fabrication of core/ shell structured SiO2/polypyrrole nanoparticles with surface modification and their electrorheology. RSC Adv 6:56495–56502

Klingenberg DJ (2007) Mason numbers for magnetorheology. J Rheol 51:883–893

Klingenberg D, Ulicny JC, Golden MA (2007) A new mason numbers for magnetorheology, proceedings of the 10th international conference on ERMR 2006 (Eds. Gordaninejad F, Graeve OA, Fuchs A, York D), pp. 94–100

Liu YD, Choi HJ (2009) Comment on "Preparation and electrorheology of new mesoporous polypyrrole/MCM-41 suspensions". J Mater Sci 44:2999–3001

Marshall L, Zukoski CF, Goodwin JW (1989) Effects of electric fields on the rheology of non-aqueous concentrated suspensions. J Chem Soc Faraday Trans 85:2785–2795

McIntyre C, Hengxi Y, Green FP (2013) Electrorheology of suspensions containing interfacially active constituents. ACS Appl Mater Interfa 5:8925–8931

Méheust Y, Parmar KPS, Schjelderupsen B, Fossum JO (2011) The electrorheology of suspensions of Na-fluorohectorite clay in silicone oil. J Rheol 55:809–833

Papanastasiou TC (1987) Flows of Materials with Yield. J Rheol 31:385–404

Parathasarathy M, Klingenberg DJ (1996) Electrorheology, mechanisms and models. Mater Sci Eng R 17:57–103

Parmar KPS, Meheust Y, Schjelderupsen B, Fossum JO (2008) Electrorheological suspensions of laponite in oil: rheometry studies. Langmuir 24:1814–1822

Sedlačík M, Mrlík M, Pavlínek V, Sáha P, Quadrat O (2012) Electrorheological properties of suspensions of hollow globular titanium oxide/polypyrrole particles. Colloid Polym Sci. 290:41–48

Seo Y (2011) A new yield stress scaling function for electrorheological fluids. J Non-Newtonian Fluid Mechan 166:241–243

Seo YP, Seo Y (2012) Modeling and analysis of electrorheological suspensions in shear flow. Langmuir 28:3077–3084

Seo YP, Choi HJ, Seo Y (2011) Analysis of the flow behavior of electrorheological fluids with the aligned structure reformation. Polymer 52:5695–5698

Seo YP, Choi HJ, Seo Y (2012) A simplified model for analyzing the flow behavior of electrorheological fluids containing silica nanoparticle-decorated polyaniline nanofibers. Soft Matter 8:4659–4663

Seo YP, Choi HJ, Seo Y (2014) Modelling and analysis of an electrorheological flow behavior containing semiconducting graphene oxide/polyaniline composite particles. Colloids Surf. A. Physicochem Eng Asp 457:363–367

Seo YP, Choi HJ, Seo Y (2015) Yield stress analysis of electrorheological suspensions containing core–shell structured anisotropic poly(methyl methacrylate) microparticles. Polym Adv Tech 26: 117–120

Seo YP, Han S, Choi J, Takahara A, Choi HJ, Seo Y (2018) Searching for a stable high-performance magnetorheological suspension. Adv Mater 30:1704769

Wu CW, Conrad H (1996) A modified conduction model for the electrorheological effect. J Phys D Appl Phys 29:3147–3153

Yamaguchi H, Zhang XR, Niu XD, Nishioka K (2010) Investigation of impulse of an ER fluid viscous damper. J Intell Mater Syst Struct 21: 423–435

Zhang M, Gong X, Wen W (2009) Manipulation of microfluidic droplets by electrorheological fluid. Electrophoresis 30:3116–3123